

# Radial migration in a bar-dominated disk galaxy I: Impact on chemical evolution

M. Kubryk<sup>1</sup>, N. Prantzos<sup>1</sup>, E. Athanassoula<sup>2</sup>

<sup>1</sup>UPMC-CNRS, UMR7095, Institut d'Astrophysique de Paris, 75014 Paris, France

<sup>2</sup>Aix Marseille Université, CNRS, LAM (Laboratoire d'Astrophysique de Marseille) UMR 7326, 13388, Marseille, France

## ABSTRACT

We study radial migration and chemical evolution in a bar-dominated disk galaxy, by analyzing the results of a fully self-consistent, high resolution N-body+SPH simulation. We find different behaviours for gas and star particles. Gas within corotation is driven in the central regions by the bar, where it forms a pseudo-bulge (disky-bulge), but it undergoes negligible radial displacement outside the bar region. Stars undergo substantial radial migration at all times, caused first by transient spiral arms and later by the bar. Despite the important amount of radial migration occurring in our model, its impact on the chemical properties is limited. The reason is the relatively flat abundance profile, due to the rapid early evolution of the whole disk. We show that the implications of radial migration on chemical evolution can be studied to a good accuracy by post-processing the results of the N-body+SPH calculation with a simple chemical evolution model having detailed chemistry and a parametrized description of radial migration. We find that radial migration impacts on chemical evolution both directly (by moving around the long-lived agents of nucleosynthesis, like e.g. SNIa or AGB stars, and thus altering the abundance profiles of the gas) and indirectly (by moving around the long-lived tracers of chemical evolution and thus affecting stellar metallicity profiles, local age-metallicity relations and metallicity distributions of stars, etc.).

**Key words:** Galaxies: abundances, Galaxies: evolution, Galaxies: ISM, Galaxies: kinematics and dynamics.

## 1 INTRODUCTION

In the past decade, observational and theoretical studies suggested that radial migration of stars may play an important role in shaping the properties of galactic disks. Already in the 1990s, it was realized that the observed dispersion in the age-metallicity relation of the solar neighborhood (Edvardsson et al. 1993) was apparently too large to be explained solely by orbital diffusion due to epicyclic motions (i.e. by stars born in the inner Galaxy, in regions of metallicity higher than the local one). Moreover, Wielen et al. (1996) argued that the Sun should have originated  $\sim 2$  kpc inwards from its current Galactocentric radius, in order to explain its high metallicity with respect to the one of the local ISM and of nearby stars; that value was close to the maximum radial epicyclic excursion  $\Delta R \sim \sqrt{2}\sigma_R/\kappa \sim 2$  kpc (in view of the observed local values of radial velocity dispersion  $\sigma_R \sim 50$  km/s (Holmberg et al. 2009) and epicyclic frequency  $\kappa \sim 37$  km/s/kpc (Binney & Tremaine 2008)). Since then, the solar metallicity has been revised downwards (Asplund et al. 2009) and it is compatible with the one of nearby young stars and of the local ISM; still, it is unclear whether observations require important radial mixing, i.e. beyond the one implied by epicyclic motions; see e.g. Nieva & Przybilla (2012) vs Haywood (2012)).

Sellwood & Binney (2002) (hereafter SB02) showed that, in the presence of recurring transient spirals, stars in a galactic disk could undergo radial displacements much larger than envisioned before: stars found at corotation with a spiral arm may be scattered to different galactocentric radii (inwards or outwards,) a process which preserves overall angular momentum distribution and does not contribute to the radial heating of the stellar disk. This development paved the way for a large number of theoretical studies on radial migration, both with numerical N-body codes and with semi-analytical models.

Lépine et al. (2003) considered a toy-model disk with corotation at a fixed galactocentric radius, removing stars locally and “kicking” them inwards and outwards. They find that in the case of the Milky Way disk, the abundance profile (assumed to be initially exponential) flattens in the 8-10 kpc region, but current data are inconclusive in that respect (Luck & Lambert 2011). Analyzing N-body+SPH simulations, Roškar et al. (2008) presented a systematic investigation of the implications of radial migration (*à la* SB02) for the chemical evolution of galactic disks; they discussed dispersion in the age-metallicity relation, broadening of the metallicity distribution, flattening of observed past abundance profiles and flattening of the observed past star formation history. Some of those effects were analyzed in more detail with a simple toy model by

Prantzos (2009), who found that the SBO2 mechanism produces an age-dependent dispersion in the age-metallicity relation (because young stars have insufficient time to migrate from far-away regions with different metallicities) and showed how the tails of the local metallicity distribution can be affected by that process.

Schönrich & Binney (2009) coupled a full chemical evolution code with a parametrized prescription of radial migration, distinguishing epicyclic motions (“blurring”) from migration (“churning”) due to transient spirals. They found excellent agreement between the results of their model and observations of the solar neighborhood and they suggested that radial mixing could also explain the formation of the Galaxy’s thick disk, by bringing to the solar neighborhood a kinematically “hot” stellar population from the inner disk. That possibility was subsequently investigated with N-body models, but controversial results are obtained up to now (compare e.g. Loebman et al. (2011) to Minchev et al. (2012)). The issue is still under debate and it is unclear whether the Galaxy’s thick disk is due to secular evolution or to the effects of past mergers e.g. (Bournaud et al. 2009; Brook et al. 2012; Forbes et al. 2012; Steinmetz 2012; Bekki & Tsujimoto 2011), while Bovy et al. (2012) suggest that the thick disk is not a distinct component of the Milky Way.

Minchev & Famaey (2010) suggested a different mechanism for radial migration than transient recurring spirals, namely resonance overlap of the bar and spiral structure; this strongly nonlinear coupling leads to a more efficient redistribution of angular momentum in the disk and produces a stellar velocity dispersion increasing with time, in broad agreement with local observations. This bar-spiral coupling was studied in detail by Shevchenko (2011) and Brunetti et al. (2011); the latter found that the extent of radial migration depends also on the kinematic state of the disk, being reduced in the case of kinematically hot disks. The radial motion of stars in disks was analyzed with N-body+SPH models for both non-barred (Grand et al. 2012b) and barred (Grand et al. 2012a) disk galaxies. By tracing particle motion around the spiral arms they showed that particles move along the arms in the radial direction, migrating towards the outer (inner) radii on the trailing (leading) side of the arm. On the other hand, Comparetta & Quillen (2012) found that radial migration may also be induced by short-lived transient density peaks (produced by interfering spiral patterns) and it may be more pervasive than that mediated by the growth and decay of long-lived individual spiral patterns. Migration due to short-lived, recurrent grand design spirals is also found in the simulations of Athanassoula (2012). Finally, the observed diversity of photometric disk profiles and, in particular, the properties of their outskirts (see Bakos et al. (2011) and references therein) have been interpreted in terms of radial migration, either fully (Roškar et al. 2008), or partially (Sánchez-Blázquez et al. 2009).

In this work, we study the implications of radial migration on the chemical evolution of a barred disk galaxy. We use a N-body+SPH simulation to study the evolution of a disk galaxy embedded in (and interacting with) a live dark matter halo of  $10^{12} M_{\odot}$ , for 10 Gyr; an early type disk galaxy with a strong bar is formed (Sec. 2). We quantify the extent of radial migration for stars and gas (Sec. 3) and we study its implications for the chemical evolution of the disk in Sec. 4. We find that, despite the important amount of radial migration occurring in our model, its impact on the chemical properties is limited. The reason is the rather flat abundance profile which is established early on in our model, due to the rapid early evolution across the whole disk.

The analysis of the results allows us to describe the radial displacement of stars in the disk in a parametrized way. We imple-

ment this parametrized description in a “traditional” detailed chemical evolution model (including long-lived sources and sinks of elements). This strategy allows us to overcome the limitations of the Instantaneous Recycling Approximation (IRA) adopted in the N-body+SPH simulation and to investigate in detail the true impact of radial migration. We find (sec. 5) that radial migration impacts on chemical evolution both directly (by affecting the age-metallicity relations, abundance profiles and metallicity distributions of stars across the disk), and indirectly, by moving around the long-lived nucleosynthesis sources and thus altering the abundance profiles of the gas; we show, in particular, how the radial profiles of O, Fe and D are affected. Our post-processing results show clearly that the full impact of radial migration on chemical evolution cannot be evaluated with numerical codes using IRA.

## 2 THE NUMERICAL SIMULATION

The simulation used in this paper was done with the GADGET3 code and it is very similar to simulation 116 described and analysed in Athanassoula et al. (2013), except that here we describe the old disk component (DISK in the standard GADGET notation) by 200 000 particles and that the softening of the halo and DISK is 100 pc (instead of 50 pc in simulation 116).

The adopted simulation has four components (HALO, DISK, GAS, STARS), having the following initial settings:

- A disk made of two initial components that are a gaseous disk (component GAS), and an old stellar disk (component DISK) having the same initial azimuthally averaged density distribution. Therefore the density distribution of the initial total disk is:

$$\rho_d(R, z) = \frac{M_d}{4\pi h^2 z_0} \exp\left(-\frac{R}{h}\right) \operatorname{sech}^2\left(\frac{z}{z_0}\right) \quad (1)$$

Where  $M_d = 5 \times 10^{10} M_{\odot}$  is the total mass of the disk (gas and old stars), the initial gas fraction is 0.75,  $h = 3 \text{ kpc}$  is the disk scale-length, and  $z_0 = 0.6 \text{ kpc}$  is the disk scaleheight. The DISK component is made of  $2.5 \times 10^5$  particles having mass  $2.5 \times 10^5 M_{\odot}$ , and has an imposed initial radial velocity dispersion of  $\sigma(R) = 100 \cdot \exp(-R/3h) \text{ km.s}^{-1}$ . The number of particles in this component remains constant during the simulation. The GAS component features  $7.5 \times 10^5$  particles having mass  $5 \times 10^4 M_{\odot}$ , which can be partially converted into new formed stars belonging to the component STARS (this one is empty at the beginning of the simulation). So the number of particles in the components GAS and STARS can change.

- A live spherical halo (component HALO) having the initial density distribution:

$$\rho_h(r) = \frac{M_h}{2\pi^{\frac{3}{2}} r_c} \frac{\alpha \exp(-r^2/r_c^2)}{r^2 + \gamma^2} \quad (2)$$

where  $M_h = 2.5 \times 10^{11} M_{\odot}$  is the halo mass,  $\gamma = 1.5 \text{ kpc}$  is the core radius,  $r_c = 30 \text{ kpc}$  is the cut-off radius. And  $\alpha = [1 - \sqrt{\pi} \exp(\gamma^2/r_c^2) (1 - \operatorname{erf}(\gamma/r_c))]^{-1}$  is a normalization factor. There are  $10^6$  particles having mass  $2.5 \times 10^5 M_{\odot}$  in the HALO component.

- The softening length is 50 pc for all components, and the opening angle for the tree-code is 0.5.

The particles in the component GAS are converted into stars with the prescriptions (including a threshold on gas volume density) given in the paper of Springel & Hernquist (2003), hereafter SH03 (see Sec. 2 and, in particular, eqs. (2) and (23) of that paper), which

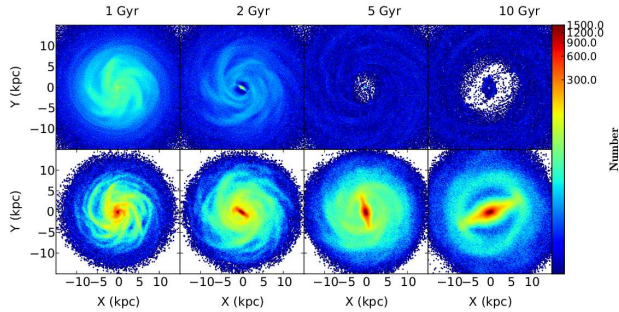


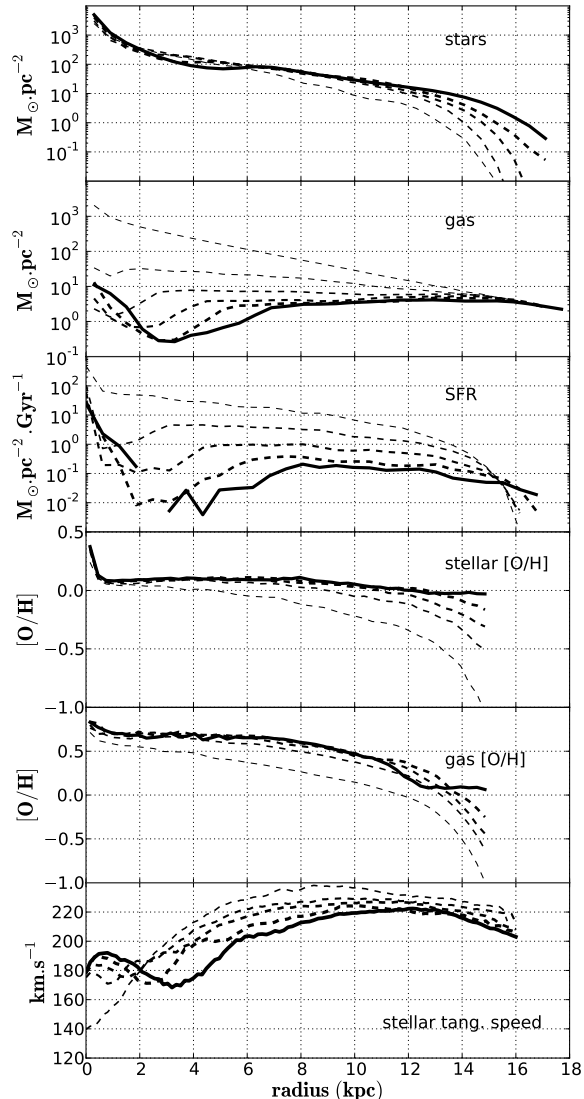
**Figure 1.** Face-on view of the simulated galaxy at 1, 2, 5 and 10 Gyr. Gas-particles are displayed in the upper row and star-particles in the lower one. The color scale on the right shows the number of particles in each pixel.

lead to a satisfactory agreement with the Schmidt-Kennicutt law. Thermal feedback is also introduced as in SH03, and the Instantaneous Recycling Approximation (IRA) is used for the chemical enrichment of the gas particles, implemented as described in Sec. 5.3 of SH03. Metal diffusion between neighbouring gas particles is not taken into account. No gas infall is considered in this simulation, i.e. the galaxy evolves as a closed box for 10 Gyr.

Some snapshots of the evolution are shown in Fig. 1. Most of the stars are formed during the first  $\sim 2$  Gyr; in that period, the gas is depleted and the disk is dominated by the presence of spiral transient structures. After 2 Gyr, a bar is formed in the center of the galaxy and grows steadily until the end of the simulation, when it extends to almost half the size of the stellar disk. The bar drives gas from the inner Lindblad resonance radius inwards. Evolving locally as in a closed box (i.e. without being replenished by infall) the gas is steadily depleted all over the disk, but more rapidly in the inner regions. Towards the end of the simulation, due to the combined action of the bar and star formation, the remaining gas is found mostly in a ring outside the bar which is separated by the central gaseous concentration by a low density annulus. The same holds for the stellar disk, which forms an inner ring (see Buta (1995) for a definition and description of inner rings).

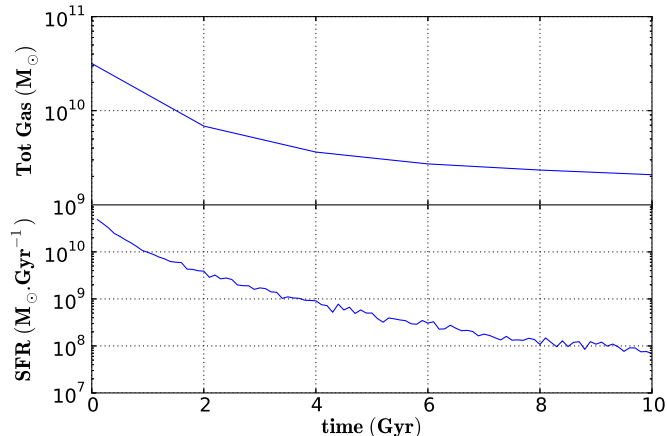
The central bar appears to be the most significant asymmetric structure in the potential, reducing the importance of spiral arms as it grows (Fig. 1). Therefore, it is expected that various dynamical phenomena linked to asymmetries in the gravitational potential (e.g. disk warming, radial migration, chaos, resonances, ...), will increasingly be consequences of the action of the bar, rather than of other structures (such as transient spiral arms).

Fig. 2 displays the evolution of the azimuthally averaged radial profiles of the surface densities of stars, gas and star formation rate, as well as of the average stellar and gas metallicities and the one of stellar tangential velocity. It should be emphasized that the average surface density profiles provide little information for the inner disk, which is dominated by the bar. The aforementioned profiles clearly reflect the inside-out formation of the disk, with the gas profiles being much more rapidly depleted in the inner disk than in the outer one, resulting in oxygen profiles becoming flatter with time. The gaseous profile is mostly depleted in the inner disk, due to both the adopted SFR law and the action of the bar which gradually produces a spoon-shaped profile. The stars at the edge of the bar can switch from almost circular orbits to elongated ones (aligned with the bar axis), thus contributing to the bar growth. Once on an elongated orbit, a star oscillates between central region and the radius of its former circular orbit. As a result, the stellar profile acquires



**Figure 2.** From top to bottom: azimuthally averaged radial profiles of the stellar surface density, gas surface density, star formation rate, average stellar and gas metallicities and rotation velocity curves. Curves correspond to snapshots taken every 2 Gyr, with the *thick solid* ones corresponding to the final (10 Gyr) result.

the same spoon-shape, and it evolves with time as the bar grows longer. The SFR profile displays similar features as the gaseous profile, as expected. The small values of the SFR outside 14 kpc result in a steep stellar profile beyond that radius. In the absence of infall, the gas is substantially depleted, only  $\sim 8\%$  of the initial quantity remaining at the end of the simulation in the whole galaxy and  $\sim 13\%$  in the disk region (outside the bar). One should notice that the final gas metallicity in the outer disk is lower than at previous epochs. This is a consequence of low-metallicity gas from the region of bar corotation region driven inwards (see also Sec. 4.1)



**Figure 3.** Evolution of the total gas amount (*top*) and of the total star formation rate (*bottom*) in the simulation.

since bar corotation is located at  $R \sim 15$  kpc towards the end of the simulation.

Fig. 3 displays the evolution of the total amount of gas (*top*) and of the star formation rate (*bottom*). Due to the adopted criteria for star formation, more than 65% of the stellar population of the galaxy is formed in the first Gyr of the evolution and approximately 85% is formed *in* the first 2 Gyr.

### 3 GLOBAL BEHAVIOR OF STAR AND GAS PARTICLES

The orbit of a test particle (star) in the potential of a galactic disk is commonly described, to first order approximation, as the superposition of a main circular motion (defining the *guiding radius*), and harmonic oscillations called epicycles. Following Sellwood & Binney (2002) we call *blurring* the radial oscillations around the guiding radius and *churning* the modifications of the guiding radius. Churning may occur through resonant interactions of the star with non-axisymmetric structures of the gravitational potential (spirals, bar), causing changes in the angular momentum of the stars. Sellwood and Binney (2002) showed that stars near corotation of a spiral perturbation may gain (lose) energy and angular momentum as they fall in the potential well of that perturbation from the leading (trailing) edge, while conserving the value of their Jacobi constant. Those changes in angular momentum make them move towards the outer (inner) disk, where they are deposited in a new quasi-circular orbit. The process conserves the overall distribution of angular momentum and does not add random motion, i.e. it does not heat the disk radially. In contrast, blurring conserves the angular momentum of individual stars but it heats radially the disk (the epicyclic radius increases with time).

In a companion paper (Kubryk et al. 2013) we analyse in some detail the behaviour of star particles undergoing churning and, in particular, the role of bar corotation and its interaction with spiral arms, in that behaviour. Here we study the impact of both churning and blurring on the chemical evolution of the disk. It is instructive to consider first the global behaviour of star and gas particles in the simulation, by plotting their initial vs. final radius (for star particles, the initial radius is their birth radius).

The results for the star particles appear in Fig. 4. Stars at a given final radius  $R_f$  originate from a large range of birth radii  $R_i$ . The distribution of  $R_i$  vs.  $R_f$  is not symmetrical with respect to the

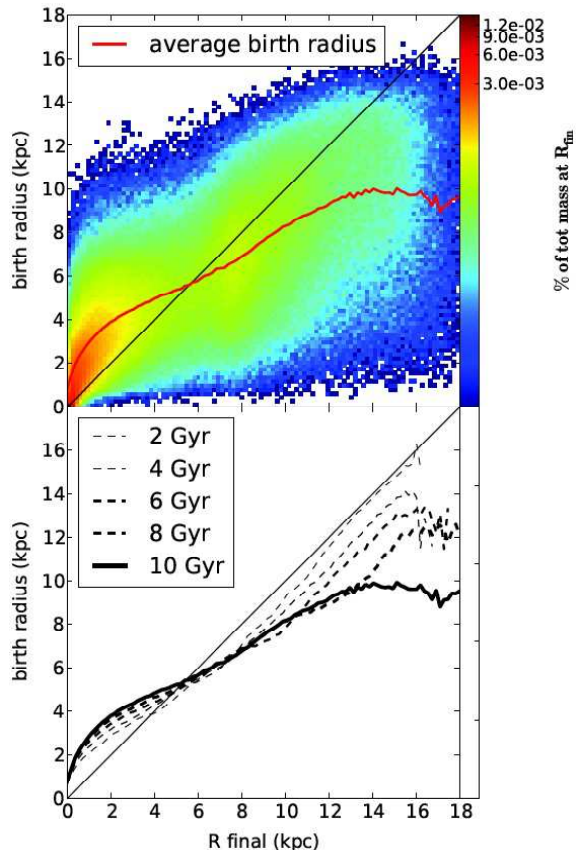


**Figure 4.** *Upper panel:* birth radius (at any time) versus final radius (at 10 Gyr) of all star-particles; the color scale represent the percentage of total stellar mass at final radius, while the red curve displays the mean birth radius of the stars at each final radius (in bins 100 pc wide). *Lower panel:* evolution of the mean birth radius of the stars at each final radius with snapshots taken every 2 Gyr and with the thickest full curve corresponding to the final time of 10 Gyr. Non-migrating stars are located on the diagonal black line (birth radius = final radius).

diagonal implying that it is not solely due to blurring (=epicyclic motion). The average ratio  $R_f/R_i$  differs significantly across the galaxy: it is smaller than 1 in the inner zones ( $R_f < 5.5$  kpc) and larger than 1 in the outer ones. Stars in the inner galaxy were born on average a couple of kpc outwards, whereas stars lying in the outer zone were born several kpc inwards. The secular evolution of the bar is responsible for the inwards movements of the stars lying inwards of 5.5 kpc at the end, because stars on initially near-circular orbits can be captured on elongated orbits at the edge of the bar, implying a mean displacement towards small radii. The steady increase of the ratio with  $R_f$  is due to the fact that there are smaller and smaller amounts of native stars as one moves to the outer disk: the corresponding average birth radius of the stellar population at  $R_f$  is then more and more affected by the population which migrated from the inner zones.

The results for gas-particles, appear in Fig. 5 (upper panel), where the birth radius of the previous figure is replaced by the initial radius since all the gas particles are present at the beginning of the simulation. In the upper panel, we distinguish two regions: inner ( $\leq 8$  kpc) and outer ( $\geq 8$  kpc) one.

In the inner region, almost all gas particles come from larger radii (there is practically no particle which has kept its original radius since the beginning). As for the stars, the inward move-

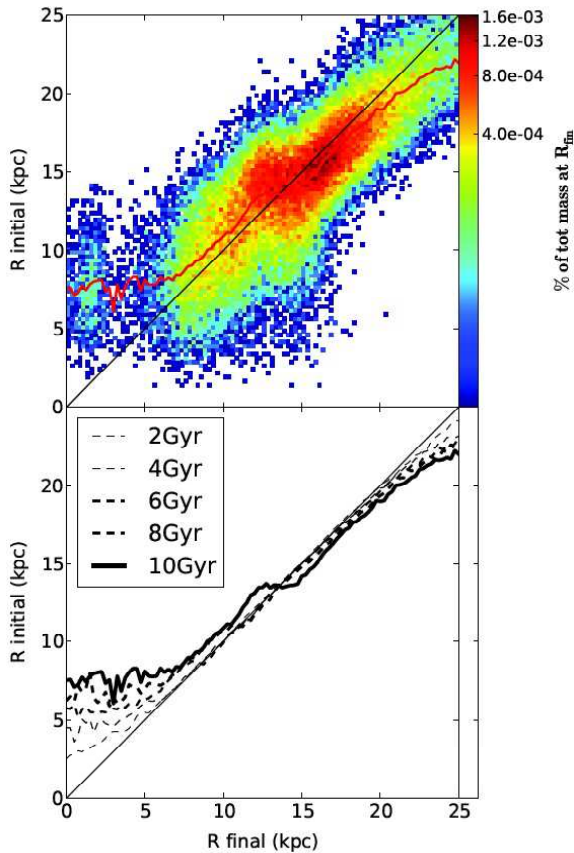


**Figure 5.** Same as in the previous figure, but for gas particles. Except that here we consider the initial radius (at  $t = 0$  Gyr), since no new gas particle appear during the simulation time.

ment of the gas particles lying in the inner zones is due to the bar (Roberts et al. (1979); Athanassoula (1992)); this gas falls to the innermost regions following orbits with an important radial component. As a result, since the gas forms a continuous fluid (contrary to the stars), the stream of falling gas creates a shock at each leading edge of the bar. The gas at radii smaller than the corotation radius, initially on circular orbits, loses energy and angular momentum each time it passes through the shock, thus it also falls towards the inner galaxy. The inflowing gas forms a small central gaseous disk (Fig. 1 and 2), where the gas density remains high enough to trigger star formation even at late times (Fig. 2). The inner galaxy is then constantly depleted of its gas by star formation and fed by the action of the bar, which brings gas from more and more large radii as the corotation moves outwards (because of the slowing down of the bar). As a result, the area between the central gaseous disk and the corotation of the bar is almost devoid of gas in the end.

In the outer regions ( $R > 6$  kpc), the gas particles are only slightly affected by the bar corotation radius: particles at radii smaller than corotation move slightly inwards ( $\leq 1$  kpc) while the ones at larger radii move slightly outwards. But the average initial radius remains close to the diagonal, around which the distribution of initial radii stays roughly symmetric.

Comparing Fig. 4 and 5, we see that both stars and gas display strong evolution in the inner regions, while only the stars display such evolution in the outer galaxy. The average displacement of gas particles in response to gravitational potential asymmetries is smaller than the one of stellar particles, because gas is a continuous dis-

sipative fluid while stars form a non-dissipative, discrete, one. The bar affects the gas mainly by driving large amounts of it to the inner regions, where they fuel star formation. Its role on the behaviour of the stellar fluid is more diverse, as will be discussed in the next sections.

## 4 CHEMICAL EVOLUTION

One of the major applications of the work of SB02 concerned the age-metallicity relation in the solar neighborhood. Using a toy model for the evolution of the metallicity profile of the Milky way disk and a probabilistic description of the radial migration, the authors showed that a large dispersion can be obtained in the local age vs.  $[\text{Fe}/\text{H}]$  relation. They found that this dispersion can be substantially larger than the corresponding observational scatter and compatible with the results of the survey of (Edvardsson et al. 1993). The seminal paper of Roškar et al. (2008) revealed other implications of radial migration, concerning the metallicity distribution and the stellar metallicity gradients in the disk.

In this section we explore the aforementioned consequences of radial migration in our barred disk model. Our investigation is limited by the use of just one metal in the numerical simulation, and by the fact that the Instantaneous Recycling Approximation has been adopted. For those reasons, standard monitors of chemical evolution like e.g. abundance ratios ( $\text{O}/\text{Fe}$  etc.) cannot be used and the results are inaccurate at late times and low gas fractions (where IRA fails to account for the late return of metal poor gas from long-lived low-mass stars). Still, it is instructive to explore some of the implications of that approximate treatment in order to get some insight into the effects of radial migration on chemical evolution.

### 4.1 The age-metallicity relation

We assume in the following that the unique metal in the simulation represents oxygen, because it constitutes almost half of the solar metallicity and because its evolution is described by IRA in a satisfactory manner in many cases, being a product of short-lived massive stars. We are fully aware that at late times IRA may over-predict oxygen abundances, but we are interested mostly in relative, not absolute, values of the abundance.

Fig. 6 (upper panel) displays the evolution of the azimuthally averaged metallicity in three different galactocentric radii, located at 4, 8 and 12 kpc, respectively. Metallicity increases rapidly in the first couple of Gyr and more slowly (less than a factor of 2 or 0.3 dex) in the remaining evolution. This applies to all radii, albeit with a small delay in the early stages, due to the inside-out formation of the disk (see 5th panel from the top in Fig. 2). The most conspicuous feature in Fig. 6 is the decline of the metallicity at 12 kpc in the last 2 Gyr of the evolution which is, in principle, unexpected. The origin of that feature is understood after inspection of Fig. 2: in the last 2 Gyr of the evolution, bar corotation is located at  $\sim 12$  kpc and drives inwards gas from the outer regions; that gas is metal poor because the metallicity profile declines rapidly outside 12 kpc (due to weak stellar activity at  $R > 12$  kpc), and dilutes the oxygen abundance at that radius while at the same time flattens the abundance profile in the region between 12 and 16 kpc.

The lower panel of Fig. 6 shows the dispersion in the gas metallicity in those same zones. Dispersion is fairly small (less than  $\sim 0.1$  dex) during the whole evolution in the 4 kpc and 8 kpc zones. In contrast, it becomes important in the 12 kpc zone in the

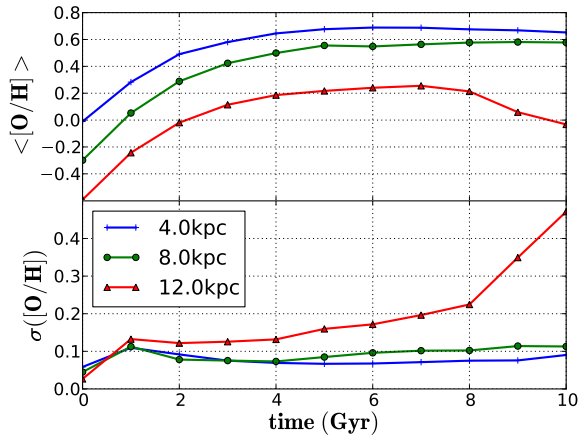


**Figure 6.** Evolution of the azimuthally averaged gas metallicity  $[O/H]$  (upper panel) and of the corresponding dispersion (in dex, lower panel) at three different galactocentric zones of width  $\Delta R=1$  kpc: 4 (solid blue), 8 (green circles) and 12 (red triangles) kpc.

last couple of Gyr, for the same reason as the decline in metallicity of that zone, namely the dilution with metal poor gas from the outer disk. This gas is driven inwards by the bar corotation and does not exchange metals with local gas, because of the simplified treatment of metals in the adopted version of the *Gadget* code. Thus, although the effect of the declining metallicity discussed in the previous paragraph is real (at least in the framework of our model), the effect of a late increasing dispersion is a numerical artifact, which impacts also on the results of the stellar metallicity dispersion as we shall see in the next paragraph<sup>1</sup>.

The stellar age-metallicity relation at 4, 8 and 12 kpc is displayed in Fig. 7, for all the stars found at 10 Gyr in those zones (left panels) and for those stars only that have been formed in those same zones (right panels). In all zones, metallicity remains flat for stars younger than 6 Gyr, as expected, because of insignificant star formation during that period. For stars born *in-situ*, dispersion is small and follows the corresponding gaseous dispersion (see Fig. 6), except in the first couple of Gyr where the gas metallicity increases rapidly: since our stellar age bins have a width of 1 Gyr, we obtain a large range of metallicity values in the first bins (and consequently a large dispersion) even though the corresponding “instantaneous” dispersion in the gas is small. It should be noticed here that the term “dispersion” has not exactly the same meaning in the case of gas and stars: for the gas, it means *instantaneous dispersion* (at any given time), but for the stars it always concerns a given *age-interval* (here taken to be of 1 Gyr); as a result, independently of any radial migration, the latter is always larger than the former: stars of age  $4(\pm 0.5)$  Gyr have a larger metallicity dispersion than the gas had 4 Gyr ago.

At late times, metallicity evolves little and *in-situ* formed stars present smaller dispersion. Radial mixing, either through churning or blurring, increases that dispersion, albeit by modest amounts. We confirm the trend originally found in SB02 of smaller dispersion with decreasing age: it is due to the fact that younger stars have

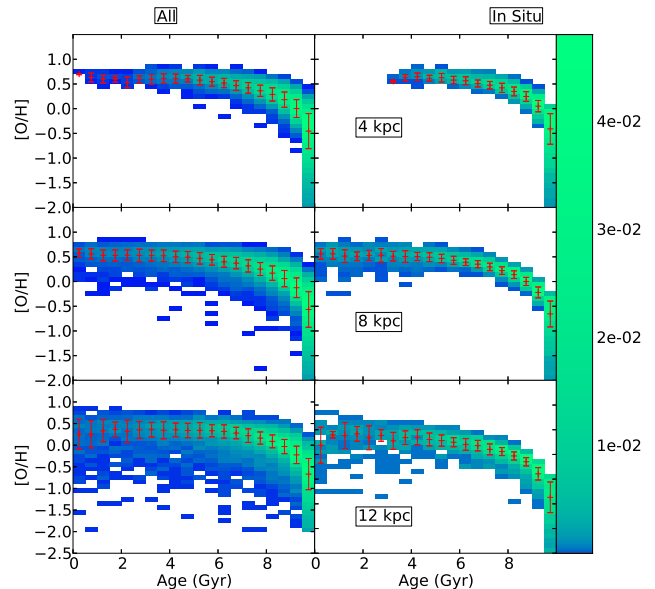


**Figure 7.** Stellar age-metallicity relation for three zones at galactocentric radii  $R=4, 8$  and  $12$  kpc, respectively (from top to bottom) and width  $\Delta R = \pm 1$  kpc. Results are displayed for all stars present in the zone at 10 Gyr (left panels) and for stars which were formed in that zone and are still there at 10 Gyr (*in-situ* stars, right panels). In all panels, at each age bin ( $\Delta(\text{Age})=1$  Gyr) the metallicity distribution is fitted by a Gaussian function, and its peak and standard deviation are displayed with (red) dots and error bars, respectively.

less time to migrate from far away regions. However, the overall effect is smaller in our case because the metallicity gradients we obtain are substantially flatter than in SB02 at all ages. At very late times, dispersion increases in the outer regions (see panels for 8 and 12 kpc), for a reason independent of radial migration: The bar corotation progressively moves outwards, driving inwards metal poor gas from the outer disk which is mixed (but not completely) with metal richer gas in the regions from 8 to 12 kpc. This is seen in Fig. 2 (the gas metallicity profile of the outer disk flattens at 10 Gyr from metal-poor gas driven inwards) and in Fig. 13 (bottom left panel, with important azimuthal variations of gas metallicity at 12 kpc). It is these variations in gas metallicity (from incomplete gas mixing from outer regions) that drive the large dispersion in stellar metallicity in the outer regions at late times.

Those results are quantitatively illustrated in Fig. 8, which shows that dispersions generally decrease with time and that the fractional dispersion difference between all the stars and the *in-situ* formed ones is also a decreasing function of time (except in the case of stars at 8 and 12 kpc, due to the aforementioned reasons).

## 4.2 Metallicity distributions

As discussed in Roškar et al. (2008), radial mixing reshuffles the metallicity distributions of stars across the disk. Our simulation shows clearly this effect, as can be seen in Fig. 9. In each one of the  $\Delta R=1$  kpc wide zones centered on 4, 8 and 12 kpc, respectively, stars born *in situ* constitute a minority at all metallicities. The stellar population at 4 kpc is dominated by stars from outer zones while those at 8 and 12 kpc are dominated by stars from the inner disk.

Due to the rapid metallicity evolution, stars originating in dif-

<sup>1</sup> We are currently implementing a considerably improved module of chemical evolution in the *GADGET* code, which contains elements from short-lived and long-lived sources - including Fe from SNIa -, and accounts for mixing of gas phases.

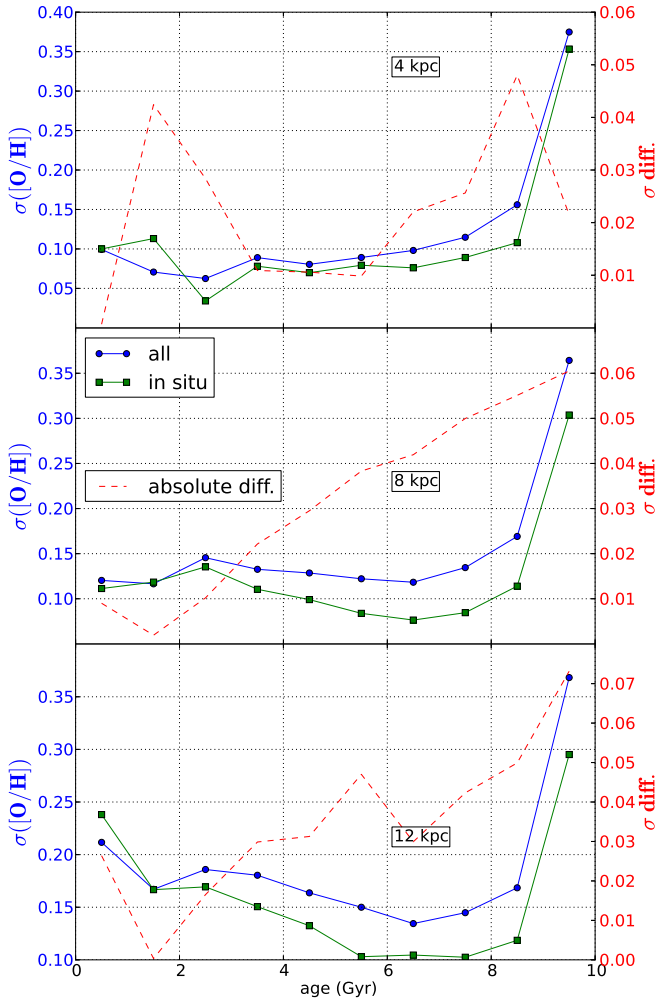


**Figure 8.** Evolution of the stellar metallicity dispersion in three zones of galactocentric radius  $R=4$ , 8 and 12 kpc and width  $\Delta R = \pm 1$  kpc. The dispersion is calculated as one standard deviation  $\sigma([O/H])$  around the mean value. The blue curves (circles) correspond to all stars present in the zone and the green curves (squares) to stars formed within the zones; both curves read on scales on the left. The red (dashed) curve represents the difference of the two others  $\sigma_{diff} = |\sigma_{all} - \sigma_{insitu}|$  and is read on the right axis.

ferent regions and ending in the same zone cover the whole metallicity range but *differ little in their average metallicity*. The small differences in the peak metallicities are explained by the fact that all zones in our model evolve practically as closed boxes, since gas particles do not suffer significant radial displacement and there is no gaseous infall. In that case the peak of the metallicity distribution corresponds to the stellar yield, e.g. (?), which is fixed in the model. The largest differences occur in the zones at 8 and 12 kpc, where stars originating in the inner and the outer zones differ, on average, by 0.1 dex in metallicity. Combined to the fact that most of those stars are formed quite early (first 2 Gyr) and have enough

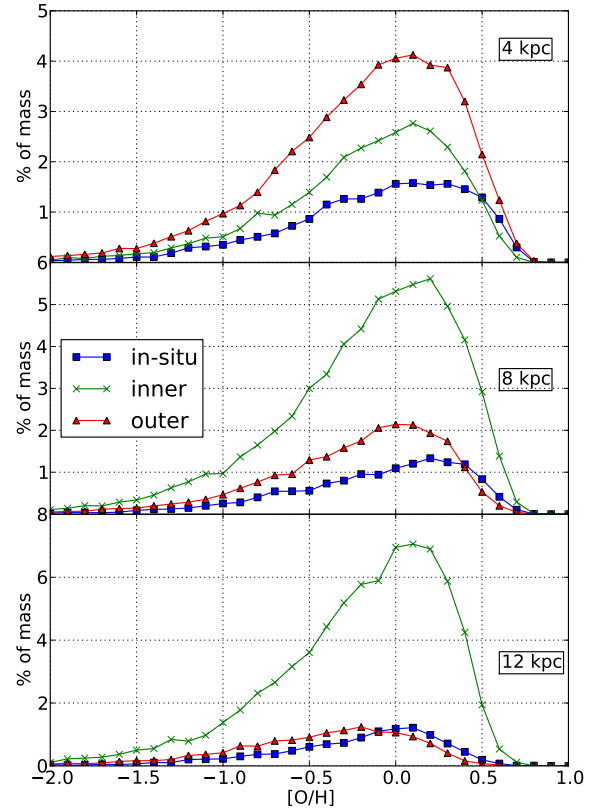


**Figure 9.** Contributions to the metallicity distributions of three radial zones ( $R=4$ , 8 and 12 kpc, from top to bottom, and width  $\Delta R = \pm 1$  kpc) from stars born *in situ* (squares and blue curves), coming from the inner galaxy (crosses and green curves) and from the outer galaxy (triangles and red curves). The width of the metallicity bins is 0.1 dex.

time to migrate all over the disk, this produces a negligible change in the peak of the metallicity distribution.

For that same reason, the width of the metallicity distributions is barely modified between stars born *in situ* and all the stars found in a given zone, as can be seen by comparing the black solid curves between left and right panels in Fig. 10. On the other hand, radial mixing does change the ratio between young and old stars in a given region, as can be seen in that same figure: as one moves outwards, from 4 to 12 kpc, the fraction of “young” stars (here defined as those younger than 7 Gyr) born *in situ* becomes more and more important with respect to the one of “old stars” (older than 9 Gyr), because of the inside-out star formation; however, if all stars are considered, then “young” stars are always a minority, even at 12 kpc (right panels in Fig. 10), because most of star formation occurs in the first couple of Gyr in our model.

### 4.3 Evolution of abundance profiles

The shape of the abundance profiles of disk galaxies constitutes a key diagnostic tool of their evolution. It has been realized long ago, with simple (independent-ring) models, that the inside-out formation of disks produces generically profiles in the gas and

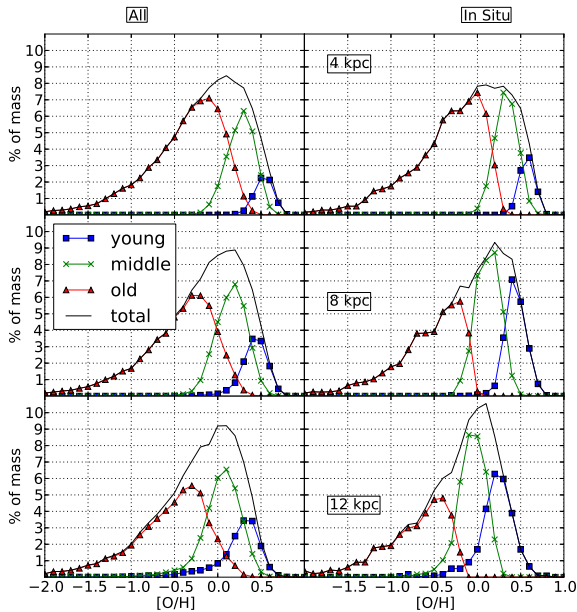


**Figure 10.** Metallicity distributions in three regions (of radius  $R=4, 8$  and  $12$  kpc, from top to bottom), for all the stars found in those zones (left) and for the stars born *in situ* (right). In each panel, three classes of stellar ages are displayed: “young” ( $<7$  Gyr, squares and blue curves), “middle-aged” ( $7-9$  Gyr, crosses and green curves) and “old” ( $>9$  Gyr, triangles and red curves); their sum (total metallicity distribution) is indicated by the black curves. The width of the metallicity bins is  $0.1$  dex.

young stars which flatten with time (Matteucci & Francois 1989; Prantzos & Aubert 1995; Boissier & Prantzos 1999; Hou et al. 2000). This was confirmed by chemo-dynamical simulations, e.g. Samland & Gerhard (2003). In a recent study comparing various codes of disk evolution for Milky Way type disks, Pilkington et al. (2012) find that: i) the gradient of oxygen may vary widely from one simulation to another, but in most cases it is substantially larger than observed in the Galaxy and ii) in most cases, the oxygen profile flattens with time.

On the basis of such considerations, it was expected that observations of stars of various ages across the disk of the MW could reveal the shape of the abundance profile as a function of time allowing one to probe the evolution of that profile and thus to draw conclusions about the local history of star formation rate vs. infall and/or radial inflows of gas. Although most studies of disk chemical evolution agree that profiles flatten with time, some models (e.g. Chiappini et al. (2001)) based on a different assumptions conclude that profiles steepen with time.

Such observations have been conducted over the years, using mostly planetary nebulae to trace the past evolution of abundance profiles. In particular, Maciel & Costa (2009) find that the abundance profile of oxygen flattens with time, thus supporting quantitatively the findings of Hou et al. (2000). However, Stanghellini & Haywood (2010) find the opposite trend, namely a steepening of oxygen profiles with time. It appears that the systematic uncertainties in ages and distances of those sources are so large at present that they do not allow for a robust evaluation of past abundance gradients. The situation may change in the future, with improvement in distance estimates and the use of proxies for the age, e.g. the  $[\alpha/\text{Fe}]$  ratio (Cheng et al. 2012).

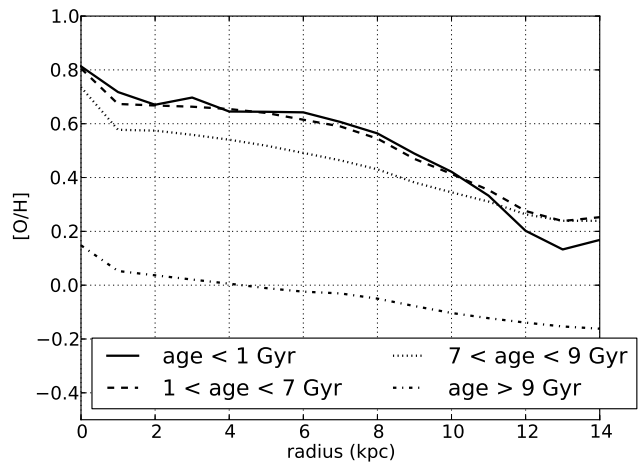


**Figure 11.** Abundance profiles of stars in various age bins. After radial mixing, profiles appear to be flatter for old stars, in contrast to what happens with the gaseous profiles.

Roškar et al. (2008) realized that one of the consequences of radial migration is to reduce and even inverse the abundance gradient of a stellar population across the galactic disk: an early steep gradient may be subsequently erased by migration of old stars towards the outer regions. Thus, even in the absence of any systematic uncertainties, abundance determinations in planetary nebulae would be of little help in revealing the past abundance profile of the disk.

We present in Fig. 11 our profiles in stars of various age bins. It can be seen that, contrary to Fig. 2, where the gas abundance profile systematically flattens with time, the stellar average abundance profile appears to be flatter for older stars. This confirms the finding of Roškar et al. (2008) and implies that even accurate observations of present days abundance profiles of stars of various ages cannot reveal the past history of the true abundance profile of the disk.

We notice, however, that the implications of this finding are not totally negative because, *in the case of a monotonic evolution of the profile*, the true abundance gradient of a stellar population at the time of its formation *should have been steeper than observed today* (since radial migration always flattens it). If the presently observed abundance profile of old stars is steeper than the one of the gas (as claimed by e.g. Maciel & Costa (2009)) then it can be safely inferred that the disk evolved from a steeper to a flatter profile. This is by itself an important conclusion, albeit in a qualitative level.

The strong early star formation of our disk galaxy leads to small early abundance gradients and thus minimizes the effects of radial migration, despite the fact that the stars have time enough (8 Gyr, on average) to migrate. Thus, the average metallicity profile of stars after the first 2 Gyr (which constitute about 90% of all stars) in our simulation has a slope of  $d\log Z/dR = -0.03$  dex/kpc. At the end of the simulation (10 Gyr) those same stars display a slope of  $-0.02$  dex/kpc, i.e. radial migration has modified the slope of the abundance profile by only  $-0.01$  dex/kpc.

In order to evaluate the effect of a steep initial metallicity profile (while keeping the same dynamical evolution) we imposed an artificial gradient of  $-0.08$  dex/kpc to all stars formed in the first 2 Gyr and we assumed that the disk evolved exactly as in our simulation. The results appear in Fig. 12 (top panel) and are compared to those of the original simulation (bottom panel). It can be seen

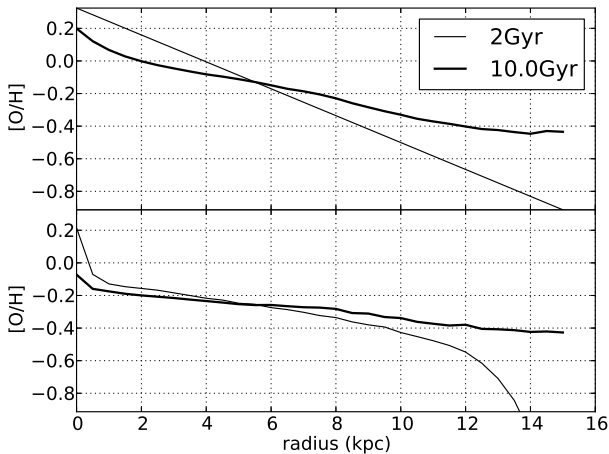


**Figure 12.** Evolution of the stellar metallicity gradient in the case of our simulation (bottom) and of the same simulation with an imposed initial gradient of  $-0.08$  dex/kpc (top). The stellar population after time  $t=2$  Gyr is displayed with thin curves in both panels; that same population, at the end of the simulation (i.e. aged of 8 Gyr) appears in thick curves.

that the slope of the final abundance profile is of  $-0.04$  dex/kpc, i.e. the same amount of radial migration modified the slope by  $-0.04$  dex/kpc, instead of  $-0.01$  dex/kpc in the original simulation. We conclude that the effect of radial migration on the final abundance profile of stars depends not only on the strength of the various churning mechanisms, but also on the overall history of the disk (star formation vs. infall and resulting chemical evolution).

#### 4.4 Azimuthal variations of metallicity

The question of azimuthal variations in either the gaseous or stellar metallicity of a disk galaxy has been addressed by various authors either from the observational (Li et al. (2013) and references therein) or from the theoretical point of view, e.g. Di Matteo et al. (2013) and references therein. In particular, Di Matteo et al. (2013) explored the possibility of azimuthal variations in old star composition as signatures of radial migration, in the case of a barred galaxy. In their controlled experiment (N-body with the SPH part switched off, i.e. no star formation) they imposed initial metallicity profiles and studied the azimuthal distribution of star particles after 4 Gyr. They found azimuthal metallicity variations depending on the initial metallicity profile and persisting during the whole period of bar activity.

Our results concerning the azimuthal metallicity of gas and stars are displayed in Fig. 13. It can be seen that in early times azimuthal variations are small in both gas and stars (0.1 dex at maximum). At late times, as the bar corotation moves outwards, metal poor gas is driven inwards from the outer disk, creating local azimuthal variations of up to 0.3 dex (a factor of 2) in the gas metallicity at 12 kpc. As already discussed for Fig. 2, this important gas inflow reduces the average radial metallicity of gas in the outer disk. However, the bulk of the stellar population in all radii is formed in early times and despite substantial radial migration it shows no significant azimuthal variations in its metallicity, because the metallicity gradient is always small. If a steep metallicity profile is imposed (as in Fig. 12) stronger azimuthal variations in

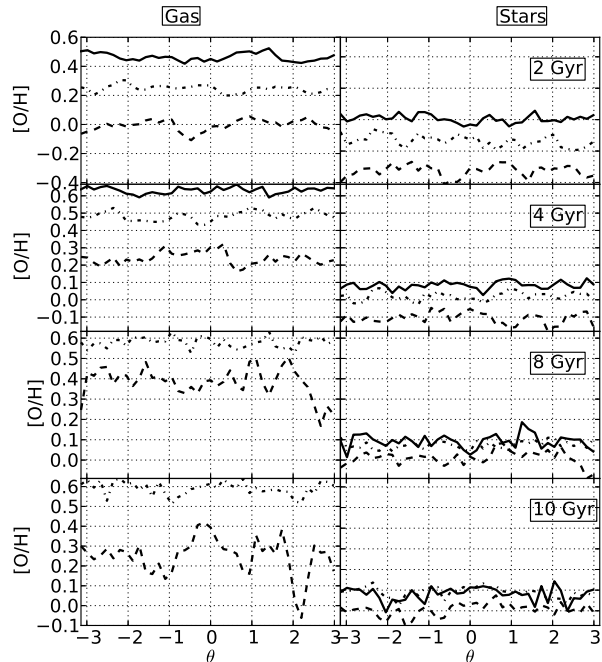


**Figure 13.** Azimuthal variations of metallicity in four different times (2, 4, 8 and 10 Gyr, from top to bottom) and in three different galactocentric distances: 4, 8 and 12 kpc (solid, dotted, dashed, respectively), for the gas (left) and for the stars (right).

the stellar population are obtained, but they never exceed the corresponding variations in the gas metallicity.

We notice that important azimuthal variations in the gas metallicity can also be obtained in the case of local infall of metal poor gas (infall is not included in our simulation). In an analogous way, a merger with a metal poor satellite could also create azimuthal variations in the stellar metallicity. For those reasons, it appears that azimuthal variations of metallicity in either gas or stars do not provide unambiguous information about radial migration.

## 5 CHEMICAL POST-PROCESSING AND THE IMPLICATIONS OF NON-IRA

As discussed in Sec. 4, the analysis of the chemical evolution part of our simulation is limited by the use of IRA and of a single metal. Here we show that it is possible to overcome this limit and gain considerable more insight, by post-processing the evolution of the simulated disk with a simple, classical model of galactic chemical evolution including a much more elaborated chemistry. In this section we first establish a parametrized description of the churning+blurring processes in the disk of our simulation. We then implement it in a classical chemical evolution model for that same galaxy, first with IRA, in order to check whether the results of the numerical simulation - which uses IRA - are satisfactorily reproduced. We show that this is indeed the case. We drop then the IRA and run the same model by introducing more chemical elements and, in particular, Fe from SNIa. This procedure allows one to exploit in detail the chemical evolution of the system (by introducing more metal sources or different prescriptions for the rates for

e.g. SNIa), once the successful description of churning+blurring through a parameterized scheme is established.

### 5.1 Parametrization of churning+blurring

Up to now, two different types of parameterization of radial mixing have been introduced in the literature. SB02 adopted a global mixing scheme, in which one assumes that a star born at radius  $R_0$  at time  $t$  may be found at time  $t_0$  (i.e. after time  $\tau = t_0 - t$ ) in radius  $R_f$  with a probability  $P(R_0, R_i, \tau)$  given by a Gaussian function

$$P(R_f, R_0, \tau) = (2\pi\sigma_\tau^2)^{-1/2} \exp\left(-\frac{(R_f - R_0)^2}{2\sigma_\tau^2}\right) \quad (3)$$

where  $\sigma_\tau$  is the 1  $\sigma$  dispersion in the radial displacement of the particles from their birth place  $R_0$  after time  $\tau$ . SB02 adopt, for illustration purposes an expression for  $\sigma_\tau$  which includes two terms accounting for churning and blurring, respectively; notice that their term for churning is not symmetric with respect to particle exchange (i.e. it depends explicitly on  $R_0$ ) but this does not have to be generically the case.

On the other hand, Schönrich & Binney (2009) treat separately blurring and churning. For the former, they make some assumptions about the radial dependence of the radial velocity dispersion of stars. For the latter, they adopt a local scheme, in which only stars from second-nearest neighboring zones can exchange places during a time-step, with a probability adjusted to reproduce some observables in the solar neighborhood, such as the metallicity distribution. According to their scheme, not only stars but also cold gas (molecular) is affected by churning. However, it seems improbable that gas - which is dissipative - behaves as the collisionless fluid of stars. Furthermore, molecular gas is bound in molecular clouds with lifetimes of only  $10^7$  yr, i.e. too short for any appreciable radial displacement. The results of our numerical simulations support these considerations, as discussed in Sec. 3 (see also Fig. 5), so we shall ignore here any radial migration of gas particles; we shall see that this approximation is valid for most of the disk, but not inside the bar, which drives rapidly gas towards the central regions.

In this work, we adopt an approach similar to the one of SB02, since their parametrization is supported by the analysis of numerical simulations by Brunetti et al. (2011) who analyzed a star-only controlled simulation performed with the Gadget-2 code. Although they had no gas or star formation in their simulation, their conditions are not very different from ours, since in our case star formation occurs essentially in the first couple of Gyr. Brunetti et al. (2011) found that the radial displacement of stars in their simulation can be described by Gaussian functions simulating a diffusion process. They caution that modeling the stellar migration as a diffusion process is valid only for time intervals less than the diffusion time-scale, which they estimate from the simulation results to be of the same order as the rotation period. In other terms, radial migration can be described as a diffusion process with diffusion coefficients depending both on time and (original) position.

We first follow the positions of all the stars of the numerical simulation born at a given radius  $R_0$  as a function of time. As displayed in Fig. 14 those stars are found at later times  $t$  at various positions  $R_t$ . The distributions of particles as a function of the position can be approximated by Gaussians with widths generally increasing as a function of time. Similar behavior characterizes the radial positions of stars born in that same radius  $R_0$  at later times or at different original radii. By constructing a sufficiently dense grid in  $R_0$  and  $t$ , we find then that the evolution of the radial dispersion

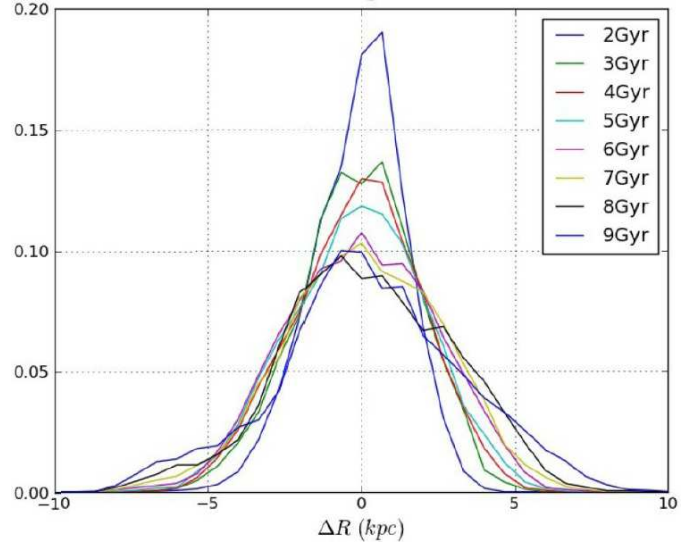


**Figure 14.** Radial positions of particles born at radius  $R_0=8\text{kpc}$  between 0 and 1 Gyr after times  $\tau$  spanning the range of 2 to 9 Gyr.

of stars can be described by expressions similar to the one of Eq. 3, where the widths are given by:

$$\sigma_\tau(R_0) = a(R_0)\tau^N + b(R_0) \quad (4)$$

Our fitting procedure produces values of  $N$  in a narrow range  $N=0.4-0.5$  at all radii and we fixed here  $N=0.5$ . Using a least square method, we get the values of  $a(R_0)$  and  $b(R_0)$  at each radius  $R_0$ :

$$a(R_0) = -6.67e^{-2}R_0 + 2.75 \quad (5)$$

$$b(R_0) = -2.26e^{-1}R_0 + 2.71 \quad (6)$$

We implement this description of radial migration in a 1D code of chemical evolution with independently evolving annuli (Boissier & Prantzos 1999). The initial configuration contains a dark matter halo of  $10^{12} M_\odot$  with a NFW profile and a gaseous disk of  $5 \cdot 10^{10} M_\odot$  with an exponential scalelength of 2.7 kpc, i.e. the same initial conditions as the N-body+SPH simulation. The disk annuli evolve as closed boxes, assuming azimuthal symmetry and IRA. The local star formation rate is assumed to be  $\Psi(R, t) = \nu \frac{V}{R} \Sigma_{Gas}^{1.5}$ , with  $\nu$  adjusted as to reproduce the final gas profile of the simulation. During a time-step  $dt$  a mass of stars  $m_S(R_0, t) = \Psi(R_0, t)dt$  is created at radius  $R_0$ . In subsequent time-steps, that mass undergoes radial migration to other zones  $R$  according to the adopted probabilistic description of Eqs. 3 and 4. Obviously, if the final profiles of gas, gas metallicity and SFR of the 1D simulation match the corresponding final profiles of the N-body+SPH simulation, the chemical evolution part of the former simulation can be considered as a successful description of the latter. And if the final profiles of stars and stellar metallicity *as well as* the initial vs. final radii of the two simulations match each other, then the adopted probabilistic description scheme can be considered as a successful description of the radial migration obtained by the N-body code.

The results of our 1D calculation appear in Fig. 15, where they are compared with those of the N-body+SPH simulation. It can be seen that, the final profiles of gas and star formation are reasonably well reproduced by the parametrized simulation, albeit with a sizable difference in the bar region (from 2 to 6 kpc). The reason for that discrepancy is that we do not consider any radial motion of the gas, an approximation which accounts well for the

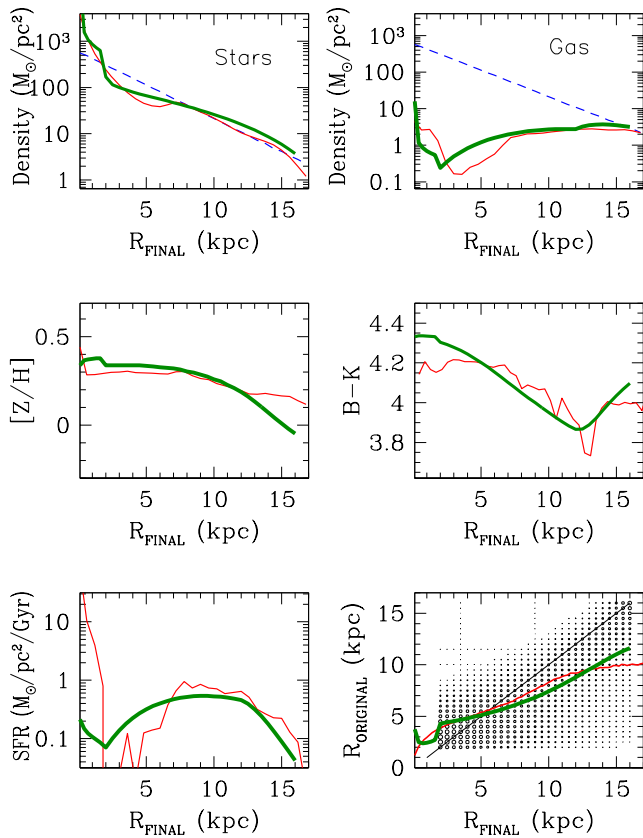


**Figure 15.** Results of the 1D chemical evolution model with IRA and parametrized description of the radial migration, as developed in Sec. 5.1, compared to those of the N-body+SPH calculation. In all panels, *thin curves* correspond to final profiles (at 10 Gyr) obtained with GADGET and *thick curves* to corresponding profiles obtained with the parametrized description and the semi-analytical model. *Top left*: Stellar surface density and *top right*: Gas surface density; in both panels the *dashed curve* corresponds to the initial gaseous profile of the disk. *Middle left*: metallicity profile; *middle right*: B-K colour profile. *Bottom left*: Star formation rate profile. *Bottom right*: Birth radius vs. final radius for all star particles (to compare with Fig. 3).

relation of  $R_0$  vs  $R_f$  of gas particles in most of the disk (see Fig. 5), but not in the region of the bar, which drives gas inwards. This also accounts for the small discrepancy of the final SFR observed in that same region. The metallicity of the gas is well reproduced over the whole disk.

The aforementioned features are obtained in the independent ring approximation adopted for the gas. The results for the final profiles of stars, stellar metallicity and colour depend also on the adopted prescription for radial migration. In Fig. 15 it is seen that over a 12 kpc region (from 3 to 15 kpc) the curves of the average initial  $R_0$  vs final  $R_f$  radius of the stars between the two simulations differ by an amount smaller than the difference between  $R_0$  and  $R_f$  in the N-body+SPH simulation (a difference which reaches almost 5 kpc in the outer disk). This suggests that the adopted description of radial migration manages to reproduce reasonably well the effect. Furthermore, the final profiles of average stellar metallicity and B-K colour are also well reproduced; in particular, we obtain the upturn of B-K around 13 kpc, as in the N-body+SPH simulation. Taking into account the extreme simplicity of our for-

mula (using Gaussian functions with a regular time dependence, while the true situation is more complicated) we consider the overall result as fairly successful.

In summary, we have shown that a simple model of galactic chemical evolution, augmented with a simplified description of radial migration *a la* SB02, can reproduce fairly satisfactorily the results of a full N-body+SPH calculation, once the diffusion coefficients have been determined from the latter simulation. This opens the way for realistic post-processing of N-body simulations, with simple chemical evolution models including many more chemical elements and nucleosynthetic sources (that were neglected in the N-body simulation). For instance, one may consider other elements than the single case of oxygen considered here, like e.g. Fe from both core collapse and thermonuclear supernovae; it is also possible to study the evolution of the system dropping IRA and considering the finite lifetimes of stars, allowing one to consider the evolution of s-elements or deuterium. We illustrate some of those possibilities in the next section.

## 5.2 Implications for chemical evolution

We run the same model as in the previous section, considering the finite lifetimes of stars as well as Fe from SNIa. We adopt the stellar lifetimes of Schaller et al. (1992), the stellar yields Woosley & Weaver (1995) and the prescription of Greggio (2005) for the rate of SNIa, which accounts for single degenerate dwarves as progenitors of those objects; each SNIa is assumed to eject 0.7  $M_\odot$  of Fe. We run the model twice: a first time without radial migration (i.e. assuming independent annuli) and a second time with radial migration.

The results of the two simulations are compared in Fig. 16, which displays the final radial profiles of various quantities obtained with radial migration *divided by* the corresponding profiles obtained without radial migration.

A first effect concerns the rate of mass ejection from long lived sources (top right panel). Radial migration depopulates the inner disk and populates the outer one with long lived (low mass) stars. In the absence of radial migration the long lived stars return lately a considerable amount of gas in the inner disk, where little gas is left and; with radial migration, a fraction of them does not return that mass in their birth place, but in the outer disk, where they migrate. However, the impact is not the same in the final gaseous profile of the inner and outer disk (top middle panel): in the inner disk, almost the totality of the gas is depleted early on from star formation, and the gas non-returned from the migrated stars is a large fraction of it; radial migration reduces the surface density of gas in the inner disk. In contrast, in the outer disk, little of the initial gas is consumed. The supplementary gas brought by the ejecta of migrated stars barely changes the overall surface density there.

The rate of oxygen ejection (middle left panel) behaves in a similar way to the rate of gas ejection (upper left panel), albeit for a non-intuitive reason: in the case of a strong early star formation (as in this simulation), most of oxygen is released at late times *not by massive stars but by the numerous intermediate and low-mass stars formed early on, which simply release their initial oxygen* (their net yield being zero, there is no chemical enrichment). In the inner regions, some of those stars are missing because of radial migration, hence less oxygen is released lately. The opposite holds for the outer regions. However, those considerations do not impact on the oxygen profile, because only the massive stars (which do not have time to migrate) enrich the local ISM with oxygen: in the inner disk radial migration reduces the local gas amount (see top middle

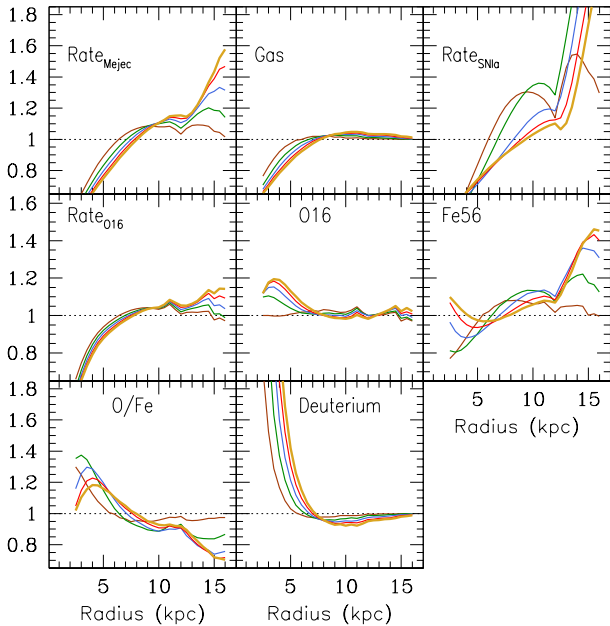


**Figure 16.** Radial profiles of various quantities obtained with radial migration *divided* by the corresponding profiles obtained without radial migration. Calculations are performed without IRA and results are displayed every two Gyr, the thickest curves corresponding to the final profiles at 10 Gyr. *First row:* Rate of mass ejection by stars, gas surface density and rate of SNIa. *Second row:* Rate of mass ejection of O-16 and gas abundance profiles of O-16 and Fe-56. *Third row:* Gas profiles of O/Fe ratio and deuterium.

panel and previous paragraph), and the dilution of the same oxygen mass in a smaller gas amount results in a larger oxygen abundance, by  $\sim 20\%$ . The effect is negligible in the outer disk.

SNIa produce a large fraction of iron in a galaxy, from one to two thirds, depending on the assumed prescription for their rate. In our case, radial migration removes a large fraction of SNIa from the inner disk and brings them in the outer disk (top right). The effect on the Fe abundance profile is straightforward in the outer disk, where Fe mass fraction is found to be  $\sim 40\%$  larger with radial migration. In the inner disk it is negligible: the missing Fe from migrated SNIa is compensated in those regions by the effect of the Fe ejected from massive star explosions being diluted in less gas (see previous paragraph for oxygen).

The effects analyzed in the previous paragraphs are summarized in the bottom left panel, displaying the O/Fe ratio: radial migration of long-lived stars (including SNIa) makes the O/Fe ratio larger in the inner disk (by up to 20%) and smaller in the outer one (by 30%). Overall, it introduces a  $\sim 50\%$  difference between the O/Fe ratios at 5 kpc and 15 kpc; this corresponds to an increase of  $\sim 0.02\text{dex/kpc}$  in the radial gradient of [O/Fe] in the gaseous phase.

Finally, in the bottom middle panel we display an interesting effect concerning the abundance of deuterium. Deuterium is produced only in the Big Bang, it is only destroyed when passing in stellar interiors (a process called astration) and most of it is astrated in the numerous low and intermediate mass stars; as a result, its abundance is steadily reduced in chemical evolution. Radial migration removes a fraction of those stars from the inner disk, hence the abundance of D in the gas of those regions is not depleted as much as in the case of no migration but remains much higher, by up to

80%. In the outer disk, the D-free gas released by the migrators has little effect, because there are considerable amounts of the initial gas, which has not been consumed by star formation. We find then that, overall, radial migration introduces an increase in the absolute value of the D gradient of  $\sim 0.025\text{ dex/kpc}$ .

## 6 SUMMARY

In this work we study the effect of radial migration on the chemical evolution of a bar-dominated disk galaxy, by analyzing a N-body+SPH simulation and using appropriately tuned semi-analytical models.

We find that the non-dissipative fluid of stars behaves differently from the dissipative fluid of gas regarding radial migration (Sec. 3): stars experience strong radial migration over the whole disk, while gas remains (on average) near its initial radius in the disk; however, in the inner galaxy, the bar transfers large amounts of gas to the central regions, affecting considerably the evolution of the developing bar/bulge. Here we focus on radial migration of stars in the disk, leaving the evolution of the bulge for a future study. By “radial migration” we mean here all types of radial displacement of stars, moving them away from their place of birth.

We studied the impact of radial migration on various aspects of the chemical evolution of the disk (Sec. 4), although our study was hampered by the use of the Instantaneous Recycling Approximation (IRA) and of a single metal (oxygen). Radial migration increases the stellar metallicity dispersion in all zones and all ages, but other factors contribute to that dispersion as well, namely the metallicity variations in the gas, due to incomplete mixing. Because of the rapid evolution in all the model zones, metallicity distributions differ little from one zone to another (their peak being close to the stellar yield), and radial migration does not change that result. On the other hand, radial migration flattens the metallicity profiles, bringing metal poor stars from the outer to the inner (metal-rich) zones and metal-rich stars from the inner to the outer (metal-poor) zones. Because of that mixing, abundance profiles of old stellar populations of a given age appear flatter from what they were at the period of stellar birth; as a consequence, their observation cannot be used to infer the true evolution of the abundance profile. The extent of that effect, however, depends a lot on the metallicity profile of the disk: if it is relatively flat at the stars’ birth, the effect will be negligible, but if it is quite steep, radial migration may not completely erase that signature. The same holds for azimuthal variations in the metallicities of gas and stars. We argue that such variations are not a safe diagnostics for radial migration, since they may have other origins (local infall of metal poor gas or a metal poor merger). Finally, we obtain a U-shaped colour profile, with old and red stars migrated from the inner to the outer disk (as already found in Roskar et al. 2008).

Because of the limitations on chemical evolution imposed by the Instantaneous Recycling Approximation adopted in the N-body+SPH simulation, we also studied the effects of radial migration on chemical evolution by adopting a different strategy. We have shown (Sec. 5) that those effects can be studied to a good accuracy by post-processing the results of a full N-body+SPH calculation with a simple chemical evolution model having detailed chemistry and a parametrized description of radial migration. We found that radial migration impacts on chemical evolution both indirectly (by affecting the age-metallicity relations and metallicity distributions of stars moved across the disk), and directly, by moving around the long-lived nucleosynthesis sources (SNIa or AGB stars of  $1.5 M_{\odot}$ )

and thus altering the abundance profiles of the gas; here (Sec. 5) we have shown how the radial profiles of O, Fe and D are affected in the case of our simulation, but other elements (like e.g. s-process elements produced in AGB stars) may be concerned as well. Our post-processing results show clearly that the full impact of radial migration on chemical evolution cannot be evaluated with numerical codes using IRA.

It should be stressed, however, that the impact of radial migration on chemical evolution depends on the system under study. Three factors have been identified up to now: strength of inhomogeneities in the gravitational potential, e.g. bar or spiral arms (stronger perturbations favoring larger effects); duration of the radial migration (the longer the bar acts, the larger the effects); and steepness of abundance profiles at the time most of the stars are formed (steeper profiles favoring larger effects). Those factors may cancel each other and mask the effects of radial migration on chemical evolution: for instance, a strong bar driving metal poor gas inwards will flatten the metallicity profile; the stars created from that gas will display quasi-similar abundances all over the disk, even in the case of strong radial migration.

This corresponds to the simulation studied here, although the reason for the flat early metallicity profile is the evolution as a closed box with a rapid early star formation. In the case of a galaxy evolving more slowly inside-out, steeper metallicity profiles are expected; however in that case, there is less time left to an average star for radial migration, so its impact on chemical evolution will not necessarily be more important. Notice that continuous infall of low metallicity gas, as expected in a galaxy like the Milky Way, should also attenuate the impact of radial migration on gas chemistry, by diluting radial abundance variations.

*Acknowledgments* E.A. acknowledges financial support by the CNES and by the European Commission through the DAGAL Network (PITN-GA-2011-289313). We are grateful to the referee for his/her thorough and constructive report.

**REFERENCES**

Asplund M., Grevesse N., Sauval A. J., Scott P., 2009, *ARA&A*, 47, 481  
 Athanassoula E., 1992, *MNRAS*, 259, 345  
 Athanassoula E., 2012, *MNRAS*, 426, L46  
 Athanassoula E., Machado R. E. G., Rodionov S. A., 2013, *MNRAS*, 429, 1949  
 Bakos J., Trujillo I., Azzollini R., Beckman J. E., Pohlen M., 2011, *Memorie della Societa Astronomica Italiana Supplementi*, 18, 113  
 Bekki K., Tsujimoto T., 2011, *ApJ*, 738, 4  
 Binney J., Tremaine S., 2008, *Galactic Dynamics: Second Edition*. Princeton University Press  
 Boissier S., Prantzos N., 1999, *MNRAS*, 307, 857  
 Bournaud F., Elmegreen B. G., Martig M., 2009, *ApJ*, 707, L1  
 Bovy J., Rix H.-W., Hogg D. W., 2012, *ApJ*, 751, 131  
 Brook C. B., Stinson G. S., Gibson B. K., Kawata D., House E. L., Miranda M. S., Macciò A. V., Pilkington K., Roškar R., Wadsley J., Quinn T. R., 2012, *MNRAS*, 426, 690  
 Brunetti M., Chiappini C., Pfenniger D., 2011, *A&A*, 534, A75  
 Buta R., 1995, *ApJS*, 98, 739  
 Cheng J. Y., Rockosi C. M., Morrison H. L., Lee Y. S., Beers T. C., Bizyaev D., Harding P., Malanushenko E., Malanushenko V., Oravetz D., Pan K., Schlesinger K. J., Schneider D. P., Simons A., Weaver B. A., 2012, *ApJ*, 752, 51

Chiappini C., Matteucci F., Romano D., 2001, *ApJ*, 554, 1044  
 Comparetta J., Quillen A. C., 2012, *ArXiv e-prints*  
 Di Matteo P., Haywood M., Combes F., Semelin B., Snaith O. N., 2013, *ArXiv e-prints*  
 Edvardsson B., Andersen J., Gustafsson B., Lambert D. L., Nissen P. E., Tomkin J., 1993, *A&A*, 275, 101  
 Forbes J., Krumholz M., Burkert A., 2012, *ApJ*, 754, 48  
 Grand R. J. J., Kawata D., Cropper M., 2012a, *MNRAS*, 426, 167  
 Grand R. J. J., Kawata D., Cropper M., 2012b, *MNRAS*, 421, 1529  
 Greggio L., 2005, *A&A*, 441, 1055  
 Haywood M., 2012, in *Assembling the puzzle of the Milky Way* Vol. 19 of *European Physical Journal Web of Conferences*, Observational constraints on the radial mixing of stars in the galactic disk. p. 5001  
 Holmberg J., Nordström B., Andersen J., 2009, *A&A*, 501, 941  
 Hou J. L., Prantzos N., Boissier S., 2000, *A&A*, 362, 921  
 Kubryk M., Athanassoula L., Prantzos N., 2013, in preparation  
 Lépine J. R. D., Acharova I. A., Mishurov Y. N., 2003, *ApJ*, 589, 210  
 Li Y., Bresolin F., Kennicutt Jr. R. C., 2013, *ApJ*, 766, 17  
 Loebman S. R., Roškar R., Debattista V. P., Ivezić Ž., Quinn T. R., Wadsley J., 2011, *ApJ*, 737, 8  
 Luck R. E., Lambert D. L., 2011, *AJ*, 142, 136  
 Maciel W. J., Costa R. D. D., 2009, in Andersen J., Nordström B., Bland-Hawthorn J., eds, *IAU Symposium Vol. 254 of IAU Symposium, Abundance gradients in the galactic disk: Space and time variations*. p. 38P  
 Matteucci F., Francois P., 1989, *MNRAS*, 239, 885  
 Minchev I., Famaey B., 2010, *The Astrophysical Journal*, 722, 112  
 Minchev I., Famaey B., Quillen A. C., Dehnen W., Martig M., Siebert A., 2012, *A&A*, 548, A127  
 Nieva M.-F., Przybilla N., 2012, *A&A*, 539, A143  
 Pilkington K., Gibson B. K., Brook C. B., Calura F., Stinson G. S., Thacker R. J., Michel-Dansac L., Bailin J., Couchman H. M. P., Wadsley J., Quinn T. R., Maccio A., 2012, *MNRAS*, 425, 969  
 Prantzos N., 2009, in Andersen J., Nordström B., Bland-Hawthorn J., eds, *IAU Symposium Vol. 254 of IAU Symposium, On the chemical evolution of the Milky Way*. pp 381–392  
 Prantzos N., Aubert O., 1995, *A&A*, 302, 69  
 Roberts Jr. W. W., Huntley J. M., van Albada G. D., 1979, *The Astrophysical Journal*, 233, 67  
 Roškar R., Debattista V. P., Quinn T. R., Stinson G. S., Wadsley J., 2008, *ApJ*, 684, L79  
 Roškar R., Debattista V. P., Stinson G. S., Quinn T. R., Kaufmann T., Wadsley J., 2008, *ApJ*, 675, L65  
 Samland M., Gerhard O. E., 2003, *A&A*, 399, 961  
 Sánchez-Blázquez P., Courty S., Gibson B. K., Brook C. B., 2009, *MNRAS*, 398, 591  
 Schaller G., Schaerer D., Meynet G., Maeder A., 1992, *A&AS*, 96, 269  
 Schönrich R., Binney J., 2009, *MNRAS*, 396, 203  
 Sellwood J., Binney J., 2002, *MNRAS*, 336, 785  
 Shevchenko I. I., 2011, *ApJ*, 733, 39  
 Springel V., Hernquist L., 2003, *MNRAS*, 339, 289  
 Stanghellini L., Haywood M., 2010, *ApJ*, 714, 1096  
 Steinmetz M., 2012, *Astronomische Nachrichten*, 333, 523  
 Wielen R., Fuchs B., Dettbarn C., 1996, *A&A*, 314, 438  
 Woosley S. E., Weaver T. A., 1995, *ApJS*, 101, 181